

The North Pacific Oscillation–West Pacific Teleconnection Pattern: Mature-Phase Structure and Winter Impacts

MEGAN E. LINKIN AND SUMANT NIGAM

Department of Atmospheric and Oceanic Science, University of Maryland, College Park, College Park, Maryland

(Manuscript received 17 May 2007, in final form 10 September 2007)

ABSTRACT

The North Pacific Oscillation (NPO) in sea level pressure and its upper-air geopotential height signature, the west Pacific (WP) teleconnection pattern, constitute a prominent mode of winter midlatitude variability, the NPO/WP. Its mature-phase expression is identified from principal component analysis of monthly sea level pressure variability as the second leading mode just behind the Pacific–North American variability pattern.

NPO/WP variability, primarily on subseasonal time scales, is characterized by a large-scale meridional dipole in SLP and geopotential height over the Pacific and is linked to meridional movements of the Asian–Pacific jet and Pacific storm track modulation. The hemispheric height anomalies at upper levels resemble the climatological stationary wave pattern attributed to transient eddy forcing. The NPO/WP divergent circulation is thermal wind restoring, pointing to independent forcing of jet fluctuations.

Intercomparison of sea level pressure, geopotential height, and zonal wind anomaly structure reveals that NPO/WP is a basin analog of the NAO, which is not surprising given strong links to storm track variability in both cases.

The NPO/WP variability is influential: its impact on Alaskan, Pacific Northwest, Canadian, and U.S. winter surface air temperatures is substantial—more than that of PNA or ENSO. It is likewise more influential on the Pacific Northwest, western Mexico, and south-central Great Plains winter precipitation.

Finally, and perhaps, most importantly, NPO/WP is strongly linked to marginal ice zone variability of the Arctic seas with an influence that surpasses that of other Pacific modes. Although NPO/WP variability and impacts have not been as extensively analyzed as its Pacific cousins (PNA, ENSO), it is shown to be more consequential for Arctic sea ice and North American winter hydroclimate.

1. Introduction

The North Pacific Oscillation (NPO) and the west Pacific (WP) teleconnection pattern constitute a prominent mode of midlatitude wintertime atmospheric variability in the Pacific basin, whose mechanisms and hemispheric climate impacts are not fully documented. The NPO is a sea level pressure (SLP) fluctuation first noted in 1916 by synoptic forecasters of the U.S. Weather Bureau (Walker and Bliss 1932). Synopticians noted that “. . . pressure variations in Hawaii were opposed to those over Alaska and Alberta, and that high pressure in Alaska meant a more southerly track of ‘lows’ and more rain in parts of the United States and

liability to cold weather east of the Rocky Mountains” (Walker and Bliss 1932, p. 57).

Being the astute climatologist that he was, Sir Gilbert Walker proposed that prevailing synoptic conditions were linked to persistent, supersynoptic (what we will refer to a subseasonal) SLP oscillations. In their monumental manuscript, Walker and Bliss pursued this notion of subseasonal variability by developing an NPO index from monthly mean SLP and surface air temperature (SAT); monthly means were constructed from daily station data. Index correlations were then used to characterize the hemispheric-wide climate response of the NPO, which included notable precipitation and SAT anomalies over North America; significant correlations were also found over Asia and South America.

A more recent analysis of the NPO is by Rogers (1981). Using the magnitude and sign of SAT anomalies between St. Paul, Alaska, and Edmonton, Canada, two phases of the NPO were defined: Aleutian below

Corresponding author address: Sumant Nigam, 3419 Computer and Space Science Bldg., University of Maryland, College Park, College Park, MD 20742-2425.
E-mail: nigam@atmos.umd.edu

(AB) and Aleutian above (AA). The AB phase of the NPO corresponds to an eastward shifted, enhanced Aleutian low, while the AA phase is just the opposite. The composite difference between the two phases is a SLP pattern nearly identical to the second eigenvector of Kutzbach (1970); the first vector was the North Atlantic Oscillation (NAO). During the eastward-shifted Aleutian low phase, eastern Siberia and the southwest United States are anomalously cold, while much of coastal and interior North America is warm, with Alaska and the Great Plains receiving more precipitation—much as in Walker and Bliss (1932). The Rogers analysis is notable for linking the NPO circulation to movements of the sea ice edge in the Bering Sea, the AB phase being associated with a southward ice edge.

While Rogers was analyzing surface climate variability, climate teleconnections were being investigated in upper-air fields. The pioneering analysis of Wallace and Gutzler (1981, hereafter WG81), which identified five major teleconnection patterns in the 500-hPa geopotential heights during northern winter, was published the same year as the Rogers paper. The west Pacific pattern, one of the five, shows strong negative correlation between centers of action at 60°N, 155°E (65°N, 170°E) and 30°N, 155°E (25°N, 165°E) in the 500-hPa height (SLP) field, the base points for the WP (NPO) index. A composite based on the 10 highest and lowest index values was used to characterize WP variability: a center over the Kamchatka Peninsula and a broad low-latitude node straddling the 155°E meridian, with a thickness pattern consistent with a cold-core equivalent-barotropic structure. More importantly, WG81 noted the WP/NPO link, writing “. . . is indicative of a close association between this pattern and the North Pacific Oscillation in the sea level pressure field identified by Walker and Bliss (1932).” A subsequent study by Barnston and Livezey (1987) extracted WP variability from rotated principal component analysis (RPCA) of 700-hPa hemispheric geopotential height anomalies. The WP pattern emerged as the second or third leading mode of variability in the 1950–84 record of monthly winter anomalies. In addition to the WP characteristics noted in WG81, an additional center of the same sign as the Kamchatka Peninsula center was found over the southwest United States in this analysis.

The vertical structure of the NPO and the WP pattern was more closely analyzed by Hsu and Wallace (1985). Their “Pacific” pattern exhibits different vertical structure over the Pacific Ocean and the Rocky Mountains. Over the Pacific, the pattern is equivalent barotropic but along the eastern slopes of the Rockies it is highly baroclinic. The structure and related circulation in the lee of the Rockies corroborates the find-

ings of Walker and Bliss (1932); higher pressure in Alaska is linked with cold air outbreaks east of the Rockies.

The monthly analysis provided valuable information on the horizontal and vertical structure of the mature-phase pattern, but little insight into the preferred variability time scale, for example, subseasonal or interannual. Esbensen’s (1984) separate analysis of intermonthly and interannual variability of 700-hPa geopotential heights showed the WP pattern to be operative on intermonthly time scales. Hsu and Wallace (1985) investigated the structure of WP variability at shorter temporal scales. They calculated lag–lead correlations of their Pacific pattern time series with the pentad-resolved 500-hPa geopotential height and SLP anomalies to gain insight into pattern evolution. Over the Rockies, they found the evolution to be different at the surface and upper-air level, with SLP anomalies moving parallel to elevation contours, but with the low-frequency Rossby wave dispersion dictating 500-hPa development.

Feldstein (2000) investigated the preferred structure of variability at even finer resolution in unfiltered daily data. His analysis of 300-hPa height anomalies shows the presence of NAO, Pacific–North American (PNA), and WP patterns, but all with *e*-folding time scales of 7–10 days, that is, close to the synoptic time scale. The NPO has also been linked to Alaskan blocking events (Renwick and Wallace 1996) and variations in the Pacific storm track (Lau 1988; Rogers 1990). The presence of these patterns in both monthly and synoptic data is interesting, meriting further investigation in the intermediate time-scale range; a weekly analysis is currently underway.

The aforementioned studies discuss WP variability largely from the circulation viewpoint. The hydroclimate impact of this height variability pattern, especially over North America, was presented in Nigam (2003), who performed teleconnection analysis on an extended record (1958–98) of winter month anomalies in the full hemispheric domain (equator–90°N), as opposed to the 15-yr (1962/63–76/77) extratropical domain (20°–90°N) analysis of WG81. A RPCA of 200-hPa heights and of SST and heights together was also performed in that study. The WP pattern was identified as the fourth leading mode of variability, behind NAO, El Niño–Southern Oscillation (ENSO), and the PNA. Linear regressions of the WP principal component on SLP and zonal winds return a SLP signature similar to the NPO, much as in WG81, and link west Pacific variability to meridional displacements of the Asian–Pacific jet. Nigam (2003) analyzed the WP links to North American precipitation and found significant correlations over the Pacific Northwest and the Great Plains, corroborating the earlier findings of Walker and Bliss (1932) and Rogers (1981).

The NPO is of course influential over the Pacific basin: Cayan (1992) found the surface heat flux associated with the NPO circulation to have a tripole structure, with consequences for sea surface temperature (SST). The NPO can also impact the Pacific trade winds since its southern lobe is located in the northern subtropics. The relaxation of trades in the weakened Aleutian low phase of the NPO is linked with ocean–atmosphere variability in the tropics/subtropics: the Pacific “Meridional Mode” (Chaing and Vimont 2004) and ENSO (Vimont et al. 2003b). The former represents interannual-to-decadal variability in the tropical basin and is driven through SST–wind coupling in the deep tropics and wind-driven SST anomalies in the northern tropics. The meridional mode was recently shown to be linked to noncanonical ENSO variability (Guan and Nigam 2008). Vimont et al. (2003a) have also argued for the importance of winter NPO SST footprints in the subtropics/tropics in stochastic forcing of the ENSO. The footprints persist and engender a coupled response according to their “seasonal footprinting” hypothesis.

The WP pattern has received little research attention in comparison with the NAO and PNA patterns and the ENSO midlatitude teleconnection. This is not surprising given the larger influence of these patterns on winter continental precipitation (Nigam 2003). The WP pattern is however, if anything, more influential in the Pacific Northwest, especially in coastal regions, in the south-central Great Plains, and, of course, on marginal sea ice zones in the Arctic. Moreover, just as the upward trend in the NAO index in recent decades spurred interest in NAO research in view of potential links with global warming, Arctic sea ice variability, especially its recent decline, is generating new interest in WP variability.

The goal of this study is to document the structure and regional climate impact of NPO/WP variability. Salient features include

- an integrated analysis of surface and upper-air variability,
- characterization of the mature-phase rotational and divergent circulations,
- NPO/WP links to Pacific storm tracks,
- NPO/WP links to Arctic sea ice concentration,
- NPO/WP links to U.S. hydroclimate and their differentiation from PNA and ENSO impacts, and
- structural correspondence of NPO/WP and NAO basin analogs?

2. Data and methodology

a. Data

The European Centre for Medium-Range Weather Forecasts (ECMWF) global reanalysis data provide

the necessary atmospheric variables for the present analysis. The global 40-yr ECMWF Re-Analysis (ERA-40; Uppala et al. 2005) spans September 1957–August 2002 and is locally available on a 2.5° latitude \times 2.5° longitude grid and 23 levels in the vertical. Monthly anomalies in the January 1958–December 2001 period are analyzed. The anomalies were computed by removing the 1958–2001 calendar month climatologies from the data.

Diabatic heating was diagnosed in house using the ERA-40 isobaric reanalyses at 2.5° resolution (S. Chan and S. Nigam 2007, unpublished manuscript). Heating was diagnosed as a residual in the thermodynamic equation (e.g., Hoskins et al. 1989; Nigam 1994), using monthly averaged data and submonthly transient fluxes, just as it was earlier for the National Centers for Environmental Prediction–National Center for Atmospheric Research (NCEP–NCAR) reanalysis and 15-yr ECMWF Re-Analysis (ERA-15; Nigam et al. 2000).

Monthly precipitation and surface air temperature data from the University of East Anglia (UEA) is used to characterize the hydroclimate impact. The global 1901–2002 station data is available on a 0.5° latitude \times 0.5° longitude grid (Mitchell and Jones 2005). Monthly SST data comes from the 1870–2002 Hadley Centre Sea Ice and SST global dataset (HadISST), on a 1° latitude \times 1° longitude grid (Rayner et al. 2003).

Sea ice concentration is generated from brightness temperature data provided by the *Nimbus-7* Scanning Multichannel Microwave Radiometer (SMMR) and Defense Meteorological Satellite Program (DMSP) F8, F11, and F13 Special Sensor Microwave Imager (SSM/I) radiances at a $25\text{ km} \times 25\text{ km}$ horizontal resolution. The product provides consistent time series of sea ice concentration as fraction (or percent) of the grid cell covered by ice. The sea ice concentration data is archived on a 1° latitude \times 1° longitude grid in polar regions at daily resolution during the January 1979–December 2004 period. The period overlapping with the ERA-40 dataset (January 1979–December 2001) is analyzed in this study. Monthly means are generated from daily sea ice data, and anomalies are computed with respect to calendar-month climatologies, as before. More information on the data is available (online at <http://www.nsidc.org/data/nsidc-0051.html>; see also Cavalieri et al. 2006).

b. Methodology

Recurrent modes of winter SLP variability are computed from covariance-based EOF analysis. Winter is defined to be the four month December–March period (DJFM). The SLP anomalies are weighted by $(\cos\theta)^{1/2}$ to account for the decrease of grid area toward the pole.

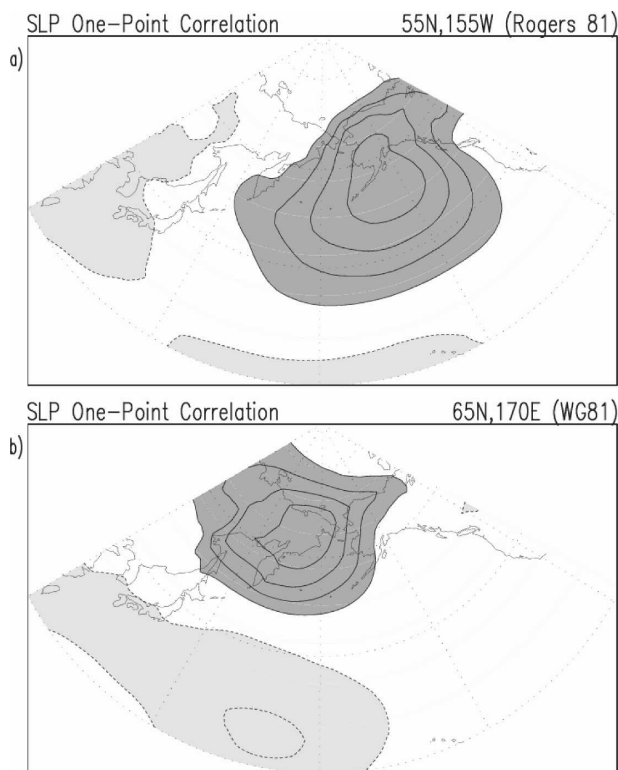


FIG. 1. One-point correlations of monthly SLP anomalies during 1958–2001 winters in the ERA-40 dataset (a) with the Rogers (1981) NPO base point and (b) with WG81's NPO base point. Base-point coordinates are noted in the upper-right corner of each plot. The contour/shading interval is 0.2 and the zero contour is suppressed. Solid (dashed) contours denote positive (negative) values.

The need for EOF rotation is obviated by confining the analysis to the Pacific basin: 20° – 85° N, 120° E– 120° W. The second principal component (PC2) of SLP is used as the NPO/WP index. Regressions of the second PC on geopotential height, zonal and meridional wind, precipitation, diabatic heating, meridional heat flux, surface air temperature, SST, and sea ice concentration are used to characterize NPO/WP variability.

3. The North Pacific Oscillation—Structure

a. SLP correlation analysis

In an attempt to connect with previous NPO studies, one-point correlation analysis is conducted on SLP anomalies. The SLP base points in Fig. 1 are 55° N, 155° W and 65° N, 170° E; the first from Rogers (1981) and the second from WG81. The correlation maps, computed using longer, more consistent records here, contain the same features as in Rogers (1981, Fig. 5) and WG81 (their Fig. 10a): a large region of positive correlation extending into eastern Alaska and western

Canada along with negative correlations to the south in the Hawaiian latitudes, with a secondary feature near Japan. The WG81 base point (65° N, 170° E) returns a qualitatively similar dipole except for the longitudinal shift. The difference between the two one-point correlation maps is likely attributable to the aliasing of PNA and ENSO influence. Both PNA and ENSO affect the North Pacific SLP in a similar manner [positive phases of each linked to lower pressure, see Nigam (2003)] and one-point correlations cannot separate these influences.¹ The meridional pressure swing manifest in these patterns is in general accord with the NPO descriptions of Rogers (1981) and Walker and Bliss (1932). Correlation patterns obtained from NCEP and ERA-40 datasets are virtually identical: only the ERA-40-based analysis will henceforth be shown.

b. EOF analysis of SLP

The second EOF describes the NPO: a meridional dipole in North Pacific SLP (Fig. 2a). The northern node has twice the magnitude of the southern one, leading to NPO's considerable influence on the position and strength of the Aleutian low. The mode explains 20.7% of the monthly winter variance in the ERA-40 SLP. The displayed EOF structure is similar to the second eigenvector of hemispheric SLP in January (Kutzbach 1970). The related circulation anomalies and thermal advection can generate high-latitude temperature anomalies consistent with the Rogers (1981) analysis.

The upper-right panel in Fig. 2 shows the second EOF from weekly SLP analysis in the same spatiotemporal domain. Not surprisingly, the amplitude is stronger now, especially of the southern lobe, but the meridional dipole structure manifest in monthly analysis is robustly returned. The variance explained by monthly and weekly modes is also nearly identical.

c. $NPO + WP = NPO/WP$

The above-described SLP variability—the NPO—is linked with the upper-air west Pacific teleconnection pattern in this section. Temporal correlation of the SLP principal component (Fig. 2e) and the WG81 WP index, spatial correlation of the SLP EOF (i.e., NPO) and the WP height pattern (Fig. 2d), and SLP regressions of the WG81 WP index (Fig. 2c) all help to make the case. The WP index is calculated from the normalized 500-hPa height anomalies at the two centers of action noted earlier, as in WG81. The temporal correlation of the

¹ The extent to which PNA variability (also subseasonal, primarily) is aliased in the Walker and Bliss (1932) NPO index is currently being investigated.

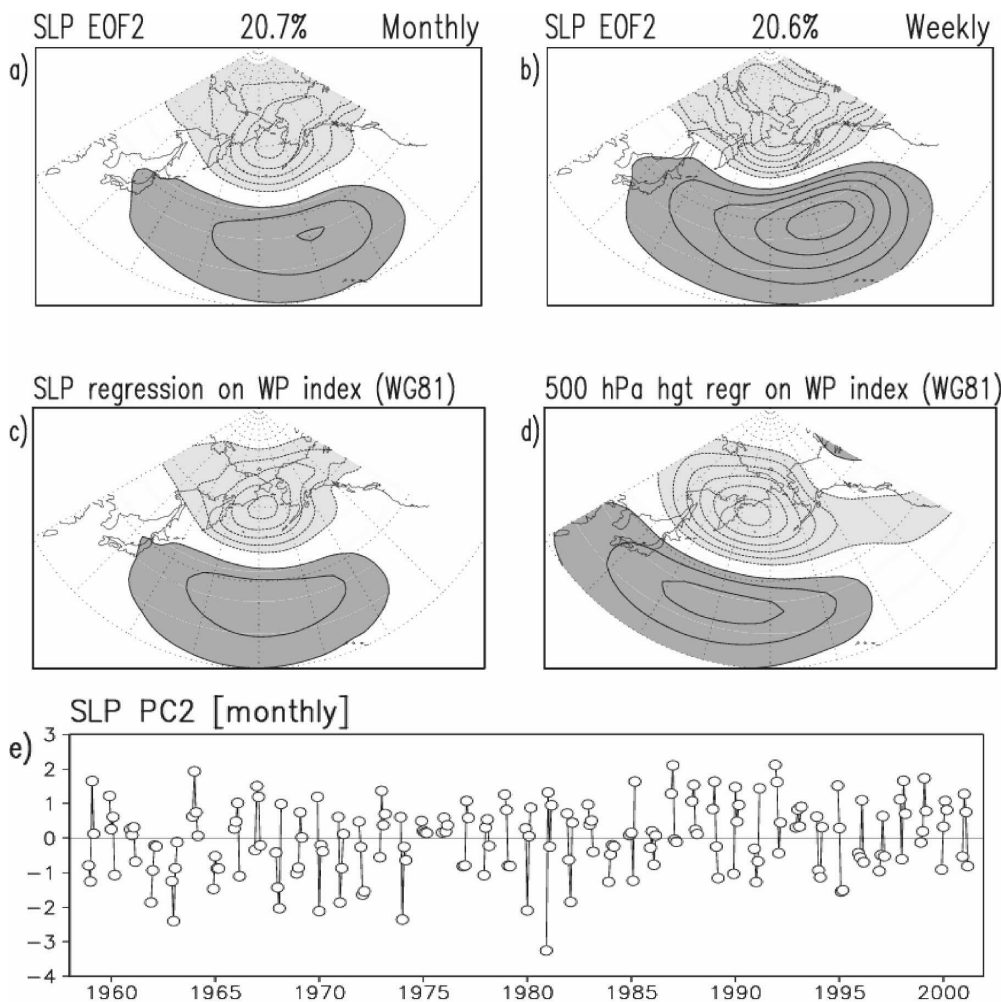


FIG. 2. Winter sea level pressure and height variability in the Pacific sector: (a) second EOF from *monthly* (DJFM) SLP analysis and (b) second EOF from *weekly* SLP analysis (17 weeks per winter); WG81's west Pacific teleconnection index regressions on (c) SLP and (d) 500-hPa geopotential height; and (e) principal component of second EOF from monthly SLP analysis; this defines our NPO/WP index. The 1958–2001 ERA-40 data are analyzed. Contour/shading interval is 1.0 hPa for SLP and 10 m for geopotential height. Solid (dashed) contours denote positive (negative) values; the zero contour is suppressed.

SLP PC and the WP index is 0.83, as is the spatial correlation of SLP EOF and the WP height pattern; both significant at the 99% level. Winter SLP regressions of the WG81 WP index (Fig. 2c) are also in remarkable agreement with the NPO (SLP EOF) structure. Given these significant temporal and spatial correlations, the North Pacific Oscillation and the west Pacific teleconnection pattern are considered to be the same mode of variability, whose SLP footprint is the NPO and whose upper-air signature is the WP teleconnection pattern. This view is reflected in our use of the NPO/WP acronym to describe this mode of winter variability in the remainder of the paper.

If the SLP PC2 is taken as marker (or index) of NPO/WP variability, one can ascertain NPO/WP links with other modes of winter variability. Given the large sub-seasonal variability, as reflected in the within-season sign change in 34 of the 44 analyzed winters, linkage with ENSO is unlikely. The small 0.16 correlation between the SLP PC and Niño-3.4 SST index confirms this to be the case. Of more interest are interbasin links in the extratropics, especially with NAO variability. Although correlation with the Hurrell (1995) NAO index is small (0.22), interbasin connection remains an interesting open issue as links may be manifest not contemporaneously, but at leads or lags. A weekly resolution

analysis will be necessary to investigate this issue, and one is in the works.

4. NPO/WP upper-air structure

The geopotential height signature of the NPO/WP at 300- and 700-hPa levels is shown in Fig. 3. In addition to the characteristic Pacific features noted earlier (e.g., Fig. 2d), the full hemispheric view shows a dual-centered ridge, whose western lobe is positioned over Canada with the eastern lobe just upstream of western Europe. This upper-air signature is consistent with the WP descriptions in literature (WG81; Horel 1981; Hsu and Wallace 1985; Barnston and Livezey 1987; Nigam 2003). Its equivalent barotropic structure is in accord with WG81's description of the pattern having a cold-core low over the Aleutians. Between the surface and 700 hPa though, there is some shift in the pattern centers: The westward tilt is slight over the North Pacific with the surface pressure anomaly centered over the western tip of Alaska and Bering Strait and the corresponding 700-hPa center positioned over eastern Siberia and the western and central Bering Sea. Over to the east, the shift is much greater. The pronounced baroclinic vertical structure over western/central North America (cf. Figs. 3b,c) has, of course, been noted before by Hsu and Wallace (1985).

Interestingly, the NPO/WP pattern bears some resemblance to the component of climatological stationary waves forced by transient fluxes of heat and momentum. Nigam and DeWeaver (2003) analyzed the forcing of these waves using a linear stationary wave model and show the response forced by orography, diabatic heating, and transient fluxes. The 300-hPa geopotential height forced by transient fluxes consists of a low over the North Pacific and a dual-centered ridge, with lobes over the Canadian Maritimes and the United Kingdom (Nigam and DeWeaver 2003, their Fig. 13d). The correspondence in features suggests that NPO/WP variability is, perhaps, linked with Pacific storm track fluctuations, a linkage investigated in the next section 5.

The vertical structure of NPO/WP variability is examined more closely in Fig. 4. A latitude–height cross section between 20° and 90°N and 1000 and 100 hPa along the 180° meridian—the longitude of maximum geopotential amplitude—is presented. The height perturbations are maximized near the tropopause, with the trough amplitude (~80 m) being twice as large as for the subtropical ridge. The temperature field is hydrostatically consistent with the height distribution: maximum warming beneath the upper-level ridge and maximum cooling in the vicinity of, but not directly underneath, the trough.

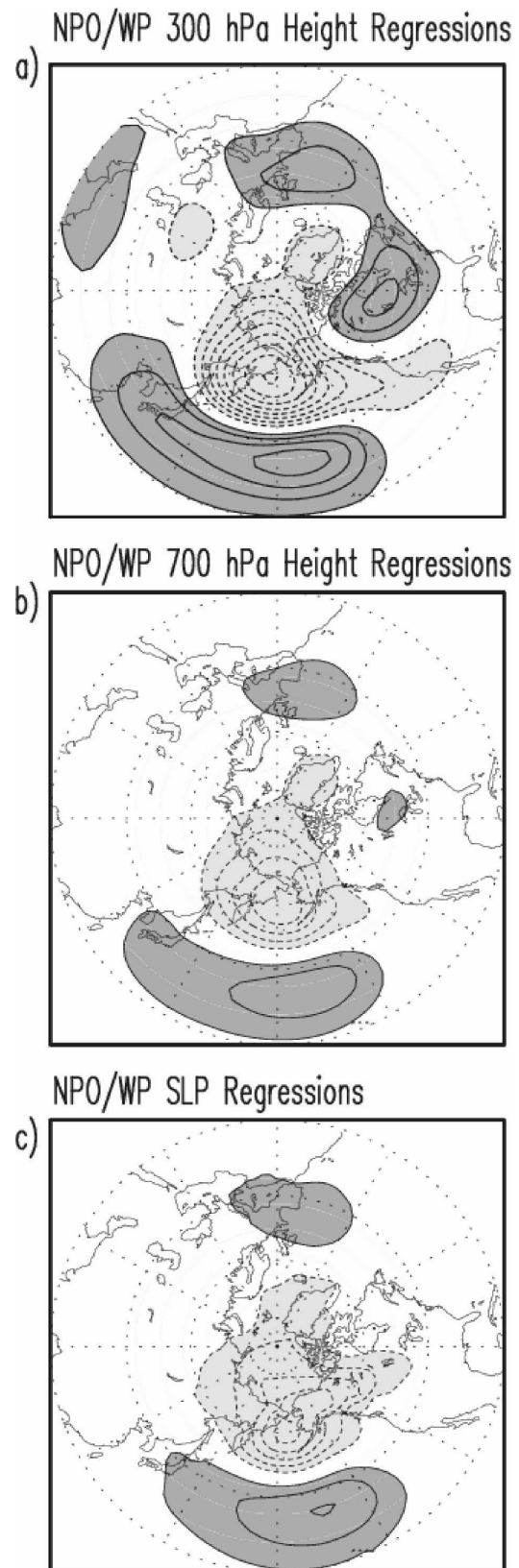


FIG. 3. NPO/WP height and SLP regressions during the 1958–2001 winter months (DJFM) for (a) 300 hPa, (b) 700 hPa, and (c) SLP. Contour/shading interval is 10 m for height and 1 hPa for SLP, and the remaining convention as before.

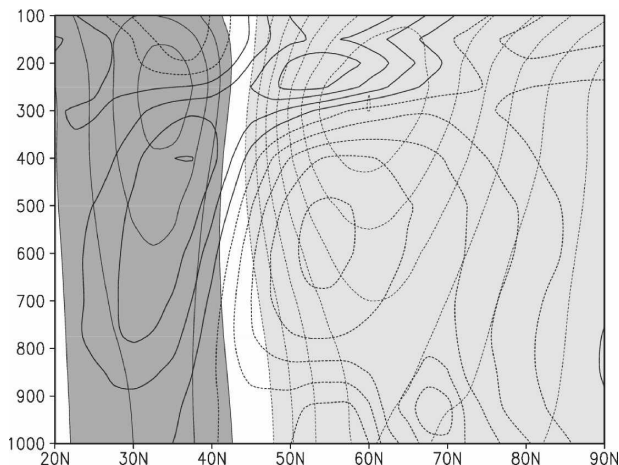


FIG. 4. NPO/WP geopotential height (shading/thin contours) and temperature (thick contours) regressions along 180° during the 1958–2001 winter months. Height is contoured at 10 m; temperature at 1-K intervals. Contour/shading convention as in Fig. 3.

Temperature in this region, in fact, displays a northward tilt with height. This feature results from the presence of cold temperatures to the south in the lower troposphere. Colder temperatures in this region must arise from zonal cold advection, originating from the NPO/WP circulation itself. The circulation consisting of anomalous westerlies here can lead to cold advection for anomalous winds coming off the cold Asian continent. The cooling is confined to the lower troposphere as the climatological land–sea thermal contrast—the basis for cold advection—is generally not evident in the middle and upper troposphere except in mountainous regions. This NPO/WP circulation-induced thermal advection results in a quadrature relationship between geopotential and temperature in the lower, but not in the upper, troposphere.

The NPO/WP zonal wind is shown atop the climatological field in Fig. 5a at 300 hPa. The wind anomaly has a meridional dipole structure and is longitudinally confined to the sector past the climatological jet core, leading to northeastward nudging of the Asian–Pacific jet in the depicted phase. Figure 5b shows the related upper-level divergence atop the zonal wind anomaly. The location of divergence features vis-à-vis the jet anomaly indicates the presence of the thermal-wind-restoring divergent circulation. The counteracting influence of this circulation on the jet anomaly suggests that the latter is likely forced by other dynamical processes (e.g., anomalous vorticity transients associated with jet displacement).

To put the NPO/WP jet fluctuation in perspective, the zonal wind anomaly associated with PNA variability is shown in Fig. 5c. This PNA anomaly is also a

meridional dipole but with a stronger southern lobe located squarely in the Asian–Pacific jet latitudes. Longitudinally, the anomaly is focused in the jet exit region, leading to an eastward extension of the jet in the depicted phase. The NPO/WP and PNA jet fluctuations are thus in near quadrature. The PNA anomalies have interesting structure in the Atlantic as well, reminiscent of the local NAO anomalies; both leading to meridional displacement of the Atlantic jet. However, different jet sectors are targeted: PNA anomalies are focused in the jet core sector, while the NAO ones are in the jet exit (and farther downstream) region (cf. following Fig. 14).

The meridional divergent circulation, which maintains thermal wind balance in response to perturbation of the Asian–Pacific jet, is shown in Fig. 6. The vertical cross section is taken along the 180° meridian, that is, at the core of the zonal wind anomalies. The divergent circulation accompanying the jet anomaly is evidently deep and thermally indirect in that rising motions occur near $\sim 60^\circ\text{N}$ while sinking takes place at $\sim 30^\circ\text{N}$. The Coriolis force owing to equatorward flow in the upper midlatitudes opposes the westerly anomaly, while related ascent (descent) to the north (south) generates adiabatic temperature changes needed to accommodate the greater vertical wind shear, that is, to restore thermal wind balance. Of particular note is the meridional location of low-level convergence just northward of the westerly anomaly core, which should be influential on cyclone storm development.²

The NPO/WP links with Pacific storm tracks are investigated in Fig. 7 using meridional wind variance, meridional heat flux, and lower-troposphere diabatic heating anomalies.³ Regressions PC2 on 300-hPa meridional wind variance display a tripole pattern with the location of the largest anomalous wind variance occurring where the climatological wind variance is largest. To its north and south, wind variance is diminished, indicating decreased cyclone activity and a narrower storm track. The NPO/WP variability is thus linked with a meridionally tighter and eastward-extended storm track. Comparison of the 700-hPa NPO/WP-related meridional heat flux (from submonthly fluctuations) with the climatological heat flux distribution (Fig. 7b) also suggests that NPO/WP variability is as-

² For discussion of the dynamical interactions between jets, divergent circulations, and storm track feedbacks, see Lau and Nath (1991) and Orlanski (2005), and references therein.

³ Submonthly variance of the unfiltered meridional wind is commonly used to monitor storm track variability (e.g., Chang 1993; Chang et al. 2002; Orlanski 2005). Other markers, such as meridional heat flux, may require bandpass filtering of data in order to focus on synoptic variability.

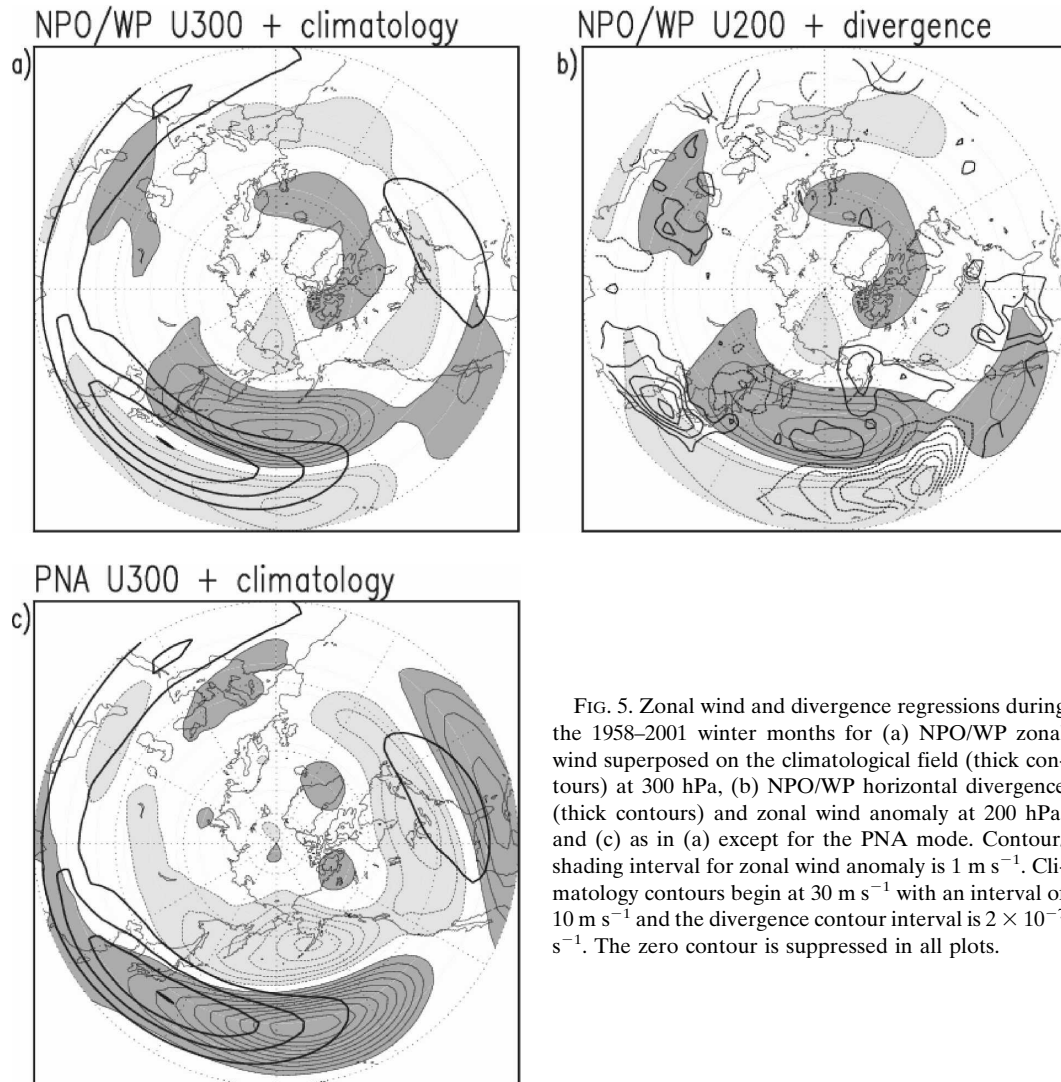


FIG. 5. Zonal wind and divergence regressions during the 1958–2001 winter months for (a) NPO/WP zonal wind superposed on the climatological field (thick contours) at 300 hPa, (b) NPO/WP horizontal divergence (thick contours) and zonal wind anomaly at 200 hPa, and (c) as in (a) except for the PNA mode. Contour/shading interval for zonal wind anomaly is 1 m s^{-1} . Climatology contours begin at 30 m s^{-1} with an interval of 10 m s^{-1} and the divergence contour interval is $2 \times 10^{-7} \text{ s}^{-1}$. The zero contour is suppressed in all plots.

sociated with a focused storm track, assuming dominance of synoptic contributions in the meridional heat flux.⁴ It is noteworthy that the Asian–Pacific jet, itself, has not strengthened since the positive NPO/WP zonal wind anomalies occur in the poleward flank of the jet (and not jet core latitudes, cf. Fig. 5a). The jet anomaly, as such, would be more consistent with meridional displacement rather than tightening/zonal extension of the storm tracks.

The NPO/WP link with lower-troposphere diabatic

⁴ The meridional heat flux is maximum slightly to the southwest of the jet anomaly core (not shown), a dynamically favored sector for synoptic development in view of the presence of a thermally direct divergent circulation, including low-level convergence, in the region upstream of the jet core. Meridional heat flux convergence is thus large poleward of the jet anomaly.

heating anomalies is displayed in Fig. 7c, with the contoured climatological heating providing positional context. The largest heating anomalies ($\sim 0.4 \text{ K day}^{-1}$) occur not where the climatological heating is a maximum, but to the northeast of this region. The climatological heating here is $1.5\text{--}2.0 \text{ K day}^{-1}$; the anomalies are thus significant. The anomalies are generated both from anomalous fluxing of cold air from the Siberian peninsula onto the warmer Pacific, leading to low-level sensible heating and, of course, from the changes in latent heating associated with storm track modulation. The lower-troposphere diabatic heating anomalies straddle the axis of maximum climatological diabatic heating, implying a meridional displacement of the storm track. This different view of storm track modulation—meridional displacement as opposed to previous indications of in-place meridional focusing—must result

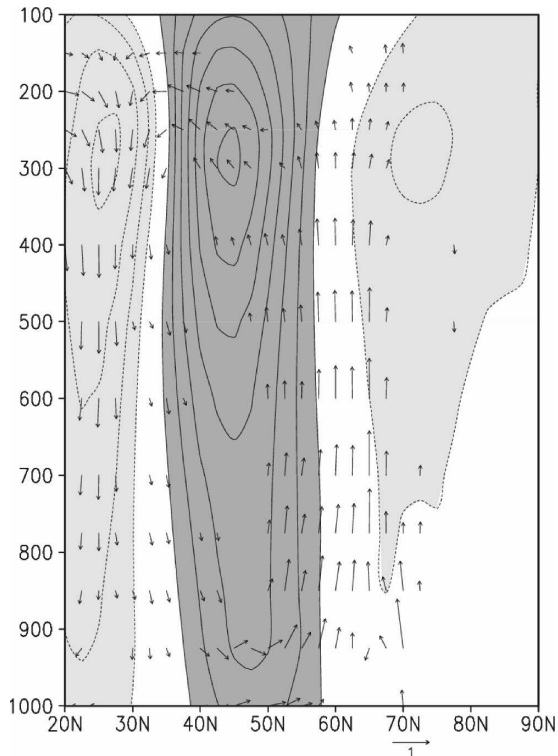


FIG. 6. NPO/WP zonal wind (contoured/shaded) and divergent circulation (vectors) along 180° during 1958–2001 winter months in ERA-40 data. Contour/shading interval for zonal wind is 1.0 m s^{-1} . The divergent wind vector ($V_x, -\omega$) is plotted after multiplying the pressure vertical velocity by -100 , using the indicated scale and when the vector magnitude exceeds 0.1 ; V_x is the divergent component of the meridional wind.

from the presence of more than just latent heating in the residual diabatic heating, for example, a sensible heating component. This will preclude characterization of storm track changes from the structure of diabatic heating anomalies.

Is the NPO/WP storm track signal manifest in direct analyses of Pacific storm track variability (e.g., Lau 1988)? Lau analyzed the bandpass- (2.5–6 day) filtered 500-hPa geopotential height variance in 19 winters (1963–81), extracting four modes of Pacific storm track variability. From PC correlations with monthly circulation and sea level pressure, Lau connected the storm track modes with monthly teleconnection patterns: the leading mode, an elongation of Pacific storm tracks (Lau's P1 mode), connected with the WP pattern and the third leading mode representing enhanced storm track activity in the eastern basin (P3), with the NPO. The distinction between WP and NPO variability is, however, untenable in view of the earlier analysis presented in this paper.

The impact of data period, variable choice, and

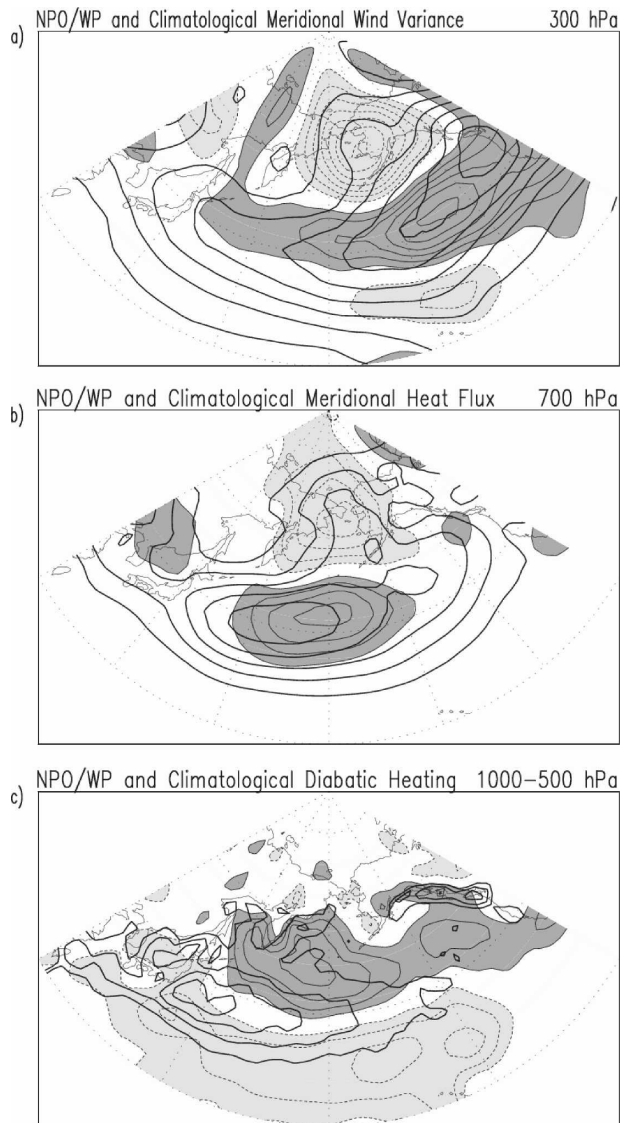


FIG. 7. NPO/WP links with Pacific storm tracks during 1958–2001 winter months in ERA-40 data shown as regressions (a) on 300-hPa submonthly meridional wind variance (contoured/shaded at $10 \text{ m}^2 \text{ s}^{-2}$) superposed on the corresponding climatology (thick contours at $50 \text{ m}^2 \text{ s}^{-2}$ interval), (b) on submonthly meridional heat flux (contoured/shaded at 1 K m s^{-1}) superposed on the corresponding climatology (thick contours at 5 K m s^{-1}) at 700 hPa, and (c) on vertically integrated (1000–500 hPa) diabatic heating (contoured/shaded at 0.1 K day^{-1}) superposed on the corresponding climatology (thick contours at 1 K day^{-1} interval; only positive values contoured to avoid confusion).

analysis pressure level differences in the two studies is currently being assessed through additional analyses. It is also conceivable that NPO/WP variability undergoes significant submonthly evolution, with different storm track links in different evolution phases—a possibility that is being actively investigated.

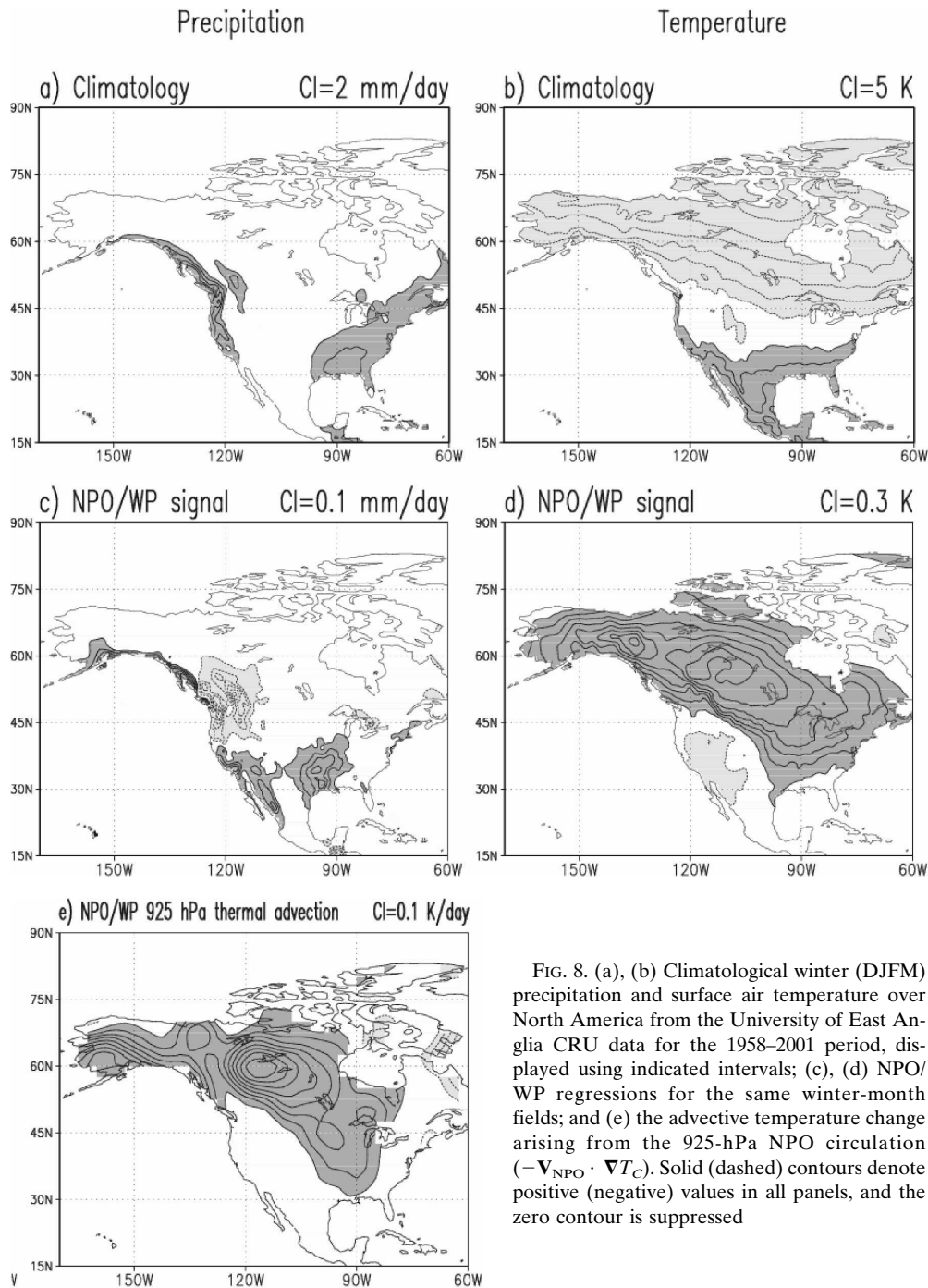


FIG. 8. (a), (b) Climatological winter (DJFM) precipitation and surface air temperature over North America from the University of East Anglia CRU data for the 1958–2001 period, displayed using indicated intervals; (c), (d) NPO/WP regressions for the same winter-month fields; and (e) the advective temperature change arising from the 925-hPa NPO circulation ($-\mathbf{V}_{\text{NPO}} \cdot \nabla T_C$). Solid (dashed) contours denote positive (negative) values in all panels, and the zero contour is suppressed

5. NPO/WP's climatic impact

The NPO/WP influence on North American climate is presented in this section through regressions on precipitation and SAT, as well as SST and sea ice. To put the influence in perspective, the winter precipitation and SAT climatology from the UEA datasets are displayed first (Fig. 8a). The Pacific Northwest gets most

of its rain in winter, with coastal regions receiving as much 14 mm day^{-1} in this high-resolution dataset. The southeast, with no preferred rainy season, on the other hand, gets $2\text{--}4 \text{ mm day}^{-1}$.

a. Precipitation

The NPO/WP enhances precipitation in coastal regions of Canada and Alaska, reduces precipitation over

the U.S. Pacific Northwest and western Canadian provinces, and enhances the same over the south-central Great Plains and western Mexico (Fig. 8c). The signal is $0.3\text{--}0.5\text{ mm day}^{-1}$ outside coastal regions where it is even stronger. A comparison with climatology indicates the NPO/WP signal corresponding to one PC unit to be, often, more than 15% of the climatology, as over south-central Great Plains and the western Canadian provinces.

The precipitation anomalies along the Alaskan/Canadian coast are also significant (NPO/WP PC precipitation correlations here are ~ 0.4) and must be due to enhanced southerly flow impinging on coastal topography and the related uplift and large-scale dynamical controls on vertical velocity.⁵ The southerly flow is enhanced along the eastern arm of the NPO/WP trough in the Aleutians (cf. Fig. 2a), leading to this dynamical influence. The precipitation decrease to the south along the U.S. Pacific Northwest coast, on the other hand, likely results from both northward displacement of the Aleutian low and from storm track displacements. The precipitation anomaly structure over the southern Great Plains is suggestive of links to the Gulf of Mexico; however, no significant circulation anomalies can be discerned in this area.

b. Surface air temperature

The SAT anomalies (Fig. 8d) result from the same circulation features discussed above. Warmer temperatures over Alaska and the Pacific Northwest, and interior central Canada, by as much as 2 K, are from thermal advection. The NPO/WP cyclonic circulation over the North Pacific positions southerly flow onto the Alaskan coast, bringing in warmer maritime air. Similarly, the ridge over North America, albeit weaker, leads to southeasterlies over much of central and western Canada, and northeasterlies to the right of the ridge bring maritime air and warmth to the eastern seaboard, especially the mid-Atlantic region. The flow becomes southeasterly moving into the Great Plains, producing the $0.4\text{--}1.2\text{ K}$ warming over the eastern and central United States. The temperature change resulting from thermal advection by the NPO/WP circulation is plot-

⁵ The operative vorticity balance on large scales is the Sverdrup balance ($\beta v \approx -\int \nabla_h \cdot \mathbf{V}$) when northward advection of planetary vorticity is balanced by horizontal convergence and upward motion. Such advection occurs along the eastern flank of the Aleutian low, leading to ascending motions and winter rainy season in the Pacific Northwest and Alaskan/Canadian coastal regions (e.g., Nigam and Ruiz-Barradas 2006). The dynamical control on vertical velocity operative in winter climatology must remain relevant during NPO/WP variability.

ted at 925 hPa in Fig. 8e. Its broad similarity with the NPO/WP temperature signal (Fig. 8d) supports the assessment regarding the advective origin of the temperature anomaly. Advection apparently explains about one-third of the amplitude with the rest accounted for by increased surface shortwave radiation (not shown).⁶ Warm advection occurs not only at the surface but also aloft, stabilizing the troposphere and decreasing cloud cover, thereby allowing more solar radiation to reach the land surface.

In the opposite phase (weakened Aleutian low), NPO/WP is associated with lower temperatures to the east of the Rockies, consistent with the propensity for cold air outbreaks in this NPO/WP phase (Walker and Bliss 1932; Rogers 1981; Hsu and Wallace 1985).

c. Sea surface temperature

The NPO/WP influence on SST is weak, but noted here in view of the spatially coherent structure of correlations, which are displayed in Fig. 9 atop the 1000-hPa wind regressions; maximum correlations are ~ 0.3 . The SST signal is apparently wind driven: In the tropics, the NPO/WP wind anomalies, especially anticyclonic flow around the southern cell, intensifies the trades in the central/eastern basin and weakens westerlies in the subtropical western basin, while cyclonic flow about the northern cell strengthens the midlatitude westerlies. The resulting wind speed and surface fluxes—stronger in the trade wind zone and midlatitudes and weaker in the subtropics—lead to SST changes: a triband anomaly structure similar to the pattern of surface heat flux anomalies linked with sea level pressure variability in the Bering Sea (Cayan 1992). SST correlations in the equatorial Pacific and Indian Ocean are weaker, but not by much. Note that only the contemporaneous SST correlations are displayed. The lagged SSTs in the Pacific, the ones leading to the “seasonal footprinting” effect (Vimont et al. 2003a), are not shown but reckoned to be important.

d. Sea ice

Arctic sea ice exhibits a rich structure of variability: an annual cycle in phase with the insolation cycle; a downward linear trend attributed to anthropogenic forcing (Solomon et al. 2007); and interannual variability driven by internal atmospheric processes (Prinsenberg et al. 1997). At the beginning of the satellite era, several studies sought to link large-scale winter atmo-

⁶ Contribution of the nonlinear ($-\mathbf{V}_{\text{NPO}} \cdot \nabla T_{\text{NPO}}$) and the other linear ($-\mathbf{V}_C \cdot \nabla T_{\text{NPO}}$) advection term has been ascertained to be small.

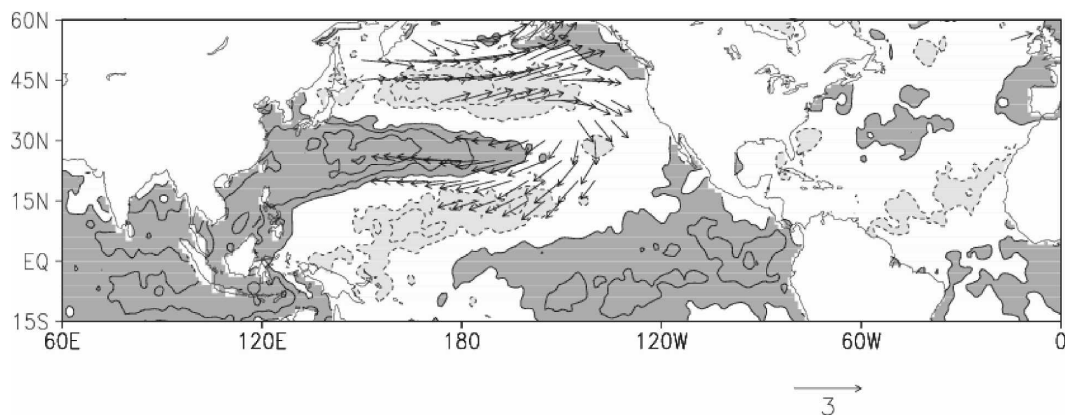


FIG. 9. NPO/WP SST correlations and 1000-hPa wind regressions during 1958–2001 winter months. SST is from the HadISST dataset while winds are from ERA-40. Wind vectors are suppressed when the wind speed is less than 0.5 m s^{-1} ; solid (dashed) contours denote positive (negative) values and the zero contour is suppressed.

spheric variability with the position of the ice edge, or marginal ice zone (MIZ). The MIZ is defined as the transition zone between the ice-free open ocean and the completely ice covered seas of the Arctic (Fang and Wallace 1994). The primary influence on the MIZ is local atmospheric variability, which results in both a dynamic and thermodynamic response. Thorndike and Colony (1982) showed that ice will drift at a 45° angle to the right of the geostrophic wind. Additionally, advection of heat into the region by cyclones or anticyclones can lead to ice melt (Pease 1980).

The MIZ and NPO/WP variabilities have been linked (Johnson 1980; Rogers 1981; Parkinson and Gratz 1983; Cavalieri and Parkinson 1987), mostly by using coarse sea ice data from satellites, including *Nimbus-7*. Many of these studies suggest that a shift in the Aleutian low results in a sea ice dipole between the Bering Sea and Sea of Okhotsk. The Rogers (1981) analysis is the most thorough from the NPO/WP perspective and concludes that the Bering Sea MIZ advances (retreats) during the positive (negative) phase of the NPO/WP.

Twenty-three years of recent sea ice concentration data are analyzed here to assess the robustness of the Rogers findings. The NPO/WP (SLP PC2) regressions are shown in Fig. 10a. The positive phase of NPO/WP variability is linked to increased ice concentration in both the Sea of Okhotsk and western Bering Sea. For reference, regressions of WG81's WP index are shown in Fig. 10b. This signal is substantially stronger in the Sea of Okhotsk and exhibits an east–west dipole in the Bering Sea. Notwithstanding some difference in emphasis, both indices are broadly in agreement in their sea ice impact in the Sea of Okhotsk and western Bering Sea.

This sea ice signal is, however, not in accord with that

described in some earlier studies, notably Rogers (1981) and Cavalieri and Parkinson (1987). Cavalieri and Parkinson found no direct link between the Sea of Okhotsk MIZ and NPO/WP variability, but found the NPO/WP negative phase (i.e., a westward-shifted Aleutian low) linked with MIZ retreat in the Bering Sea. Likewise, Rogers (1981) did not firmly link the NPO/WP and MIZ position in the Sea of Okhotsk, only suggesting that sea ice concentration decreased during the positive NPO/WP phase (an eastward-shifted, intensified Aleutian low), that is, opposite of our finding.

Although the strategy is similar, our analysis of a longer period, more consistent sea ice record leads to contradictory findings: The MIZ does advance southward in the western Bering Sea during the NPO/WP positive phase, increasing ice concentration by as much as 10%. The MIZ response is, however, not uniform as there is little impact in the eastern Bering Sea. A robust signal is, additionally, found in the Sea of Okhotsk where ice concentration increases by as much as 8% during the positive NPO/WP phase. These increments are twice as large as the PNA-related sea ice increase in the Bering Sea and Sea of Okhotsk (not shown).

Given that the NPO/WP influence on sea ice is quite different in our analysis, it is important to assess the dynamical and thermodynamical consistency of the sea ice variability pattern with the overlying circulation. The 1000-hPa NPO/WP circulation (SLP and wind vectors) and resulting horizontal thermal advection are displayed in Fig. 11. Westerly to west-northwesterly winds and cold air advection prevail over much of the Sea of Okhotsk and result in sea ice formation and ice drift away from the Russian coastline, thus increasing ice concentration in the Sea of Okhotsk. Similarly, northerly winds and cold air advection are linked with sea ice

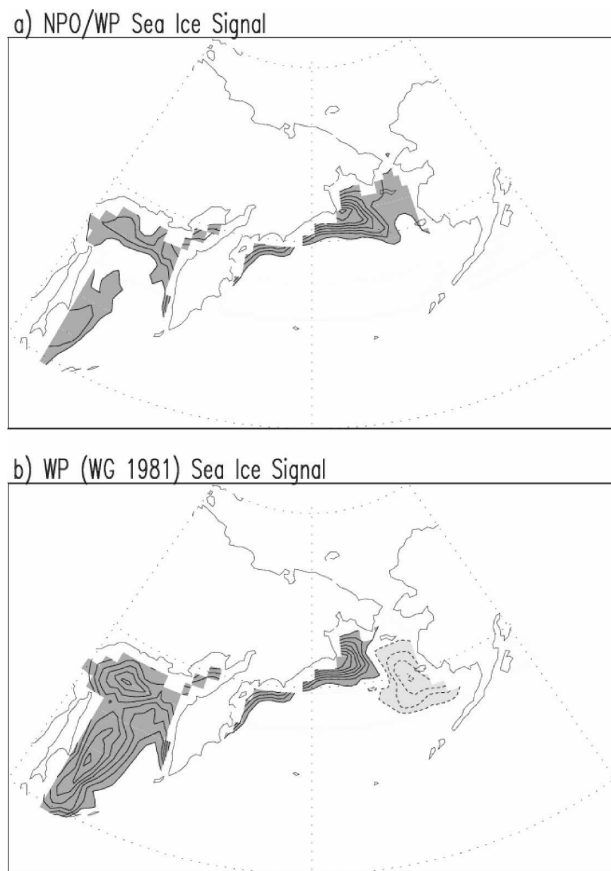


FIG. 10. Regressions on Sea of Okhotsk and Bering Sea ice concentration during the 1979–2001 winter months (DJFM) for (a) NPO/WP and (b) the WG81 WP index. Contour/shading interval for ice concentration is 1%; solid (dashed) contours denote positive (negative) values, and the zero contour is suppressed.

increase in the western Bering Sea. Anomalous flow in the eastern Bering Sea is, however, from the south to southeast direction, leading to warm air advection in that region. Interestingly, no significant ice decrease is evident in that region (cf. Fig. 10a), but there is no increase either. The WP index (WG81) regressions however do show a decrease of ice in the eastern Bering Sea, but this does not lessen the inconsistency between circulation and sea ice patterns of the NPO/WP index.

Sea ice variability also arises from sea ice motion, which is influenced by a number of factors including proximity of sea ice to the coast and the direction of prevailing winds relative to the coastline (Fissel and Tang 1991). Both the Bering Sea and Sea of Okhotsk are bordered by land on multiple sides, which complicates the analysis of motion-induced sea ice variability. Internal ice dynamics introduces additional complexity, making the sea ice response to wind forcing dependent on local ice thickness: Thinner ice (lower internal

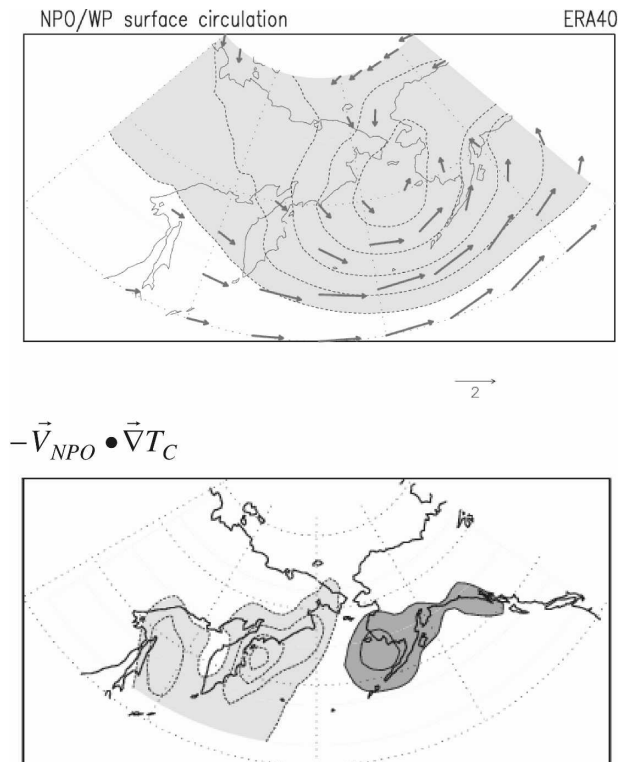


FIG. 11. (top) NPO/WP SLP and 1000-hPa wind regressions during 1958–2001 winter months and (bottom) 1000-hPa horizontal temperature advection by the NPO/WP circulation. Wind vectors are suppressed when the wind speed is less than 1 m s^{-1} ; SLP is contoured at 1 hPa and thermal advection at 0.4 K day^{-1} interval; solid (dashed) contours denote positive (negative) values, and the zero contour is suppressed in both panels.

stress) and lower sea ice concentration regions respond more strongly to atmospheric forcing (Schevchenko et al. 2004). These impacts, not considered here, could account for the pending inconsistency between the NPO sea ice signal and related atmospheric thermodynamic forcing (cf. Figs. 10a and 11b).

6. Comparison with PNA and ENSO

It is interesting and, perhaps, also important to differentiate the NPO/WP structure and impacts with those of PNA and ENSO variability, as the Pacific sector is home to all three variability modes. The SLP signature of PNA variability (EOF1) is displayed in Fig. 11a while that of ENSO variability is shown in Fig. 11b; the ENSO signature is obtained from Niño-3.4 SST index regressions. Clearly, via constraints imposed by EOF analysis, the PNA and NPO/WP variability are uncorrelated, both temporally and spatially. Close inspection of the SLP patterns (cf. Figs. 2a and 12a) shows the PNA signal to be maximal near the nodal line

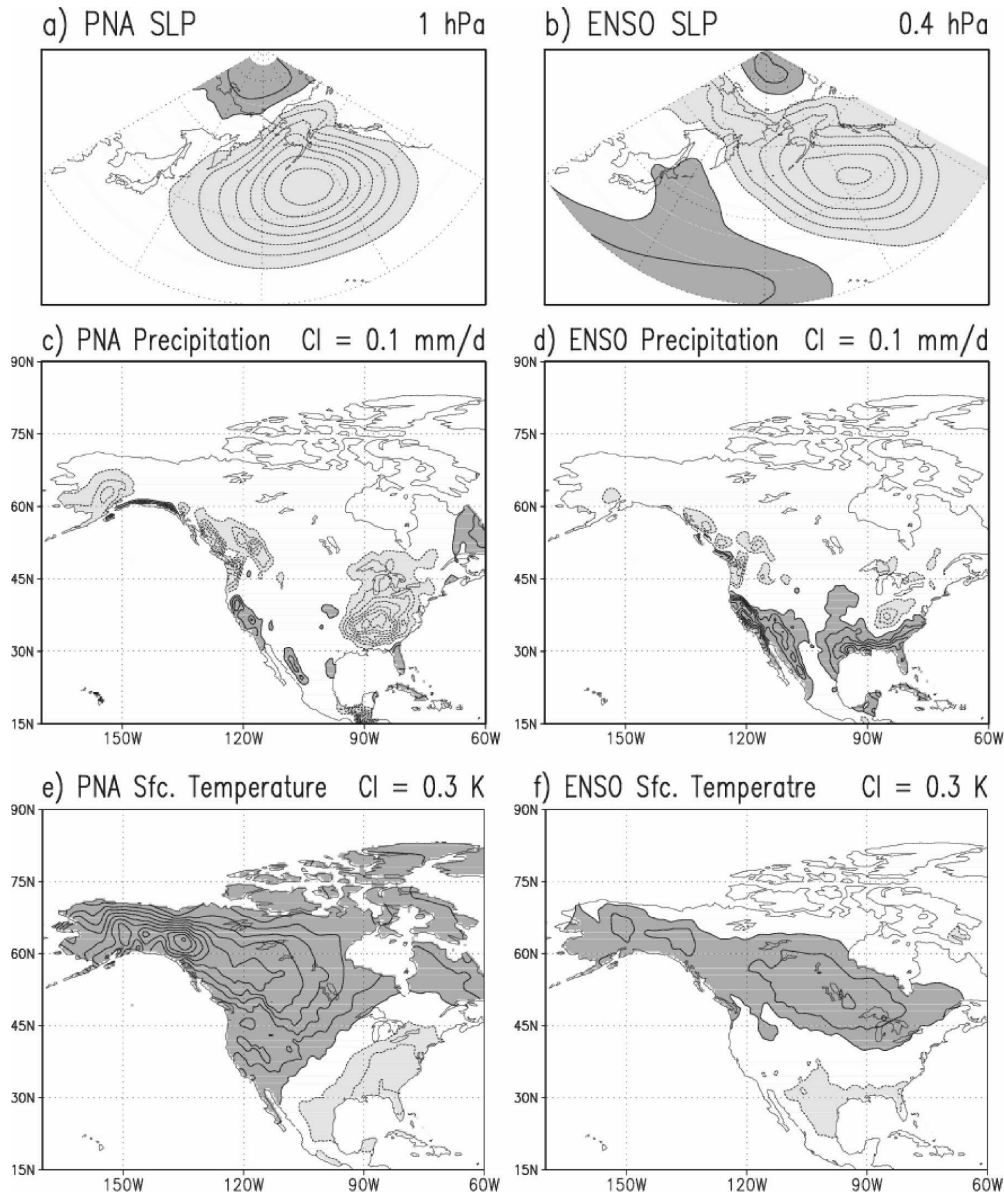


FIG. 12. Winter (top) sea level pressure, (middle) precipitation, and (bottom) surface air temperature patterns associated with PNA and ENSO variability. PNA anomalies are diagnosed from regressions of the leading PC of monthly SLP analysis (the second mode of which is NPO/WP) and ENSO anomalies are obtained from Niño-3.4 SST index regressions; both are for the 1958–2001 winter months. Contour/shading interval is 1.0 hPa for the PNA SLP, 0.4 hPa for ENSO SLP, 0.1 mm day⁻¹ for precipitation, and 0.3 K for temperature. Solid (dashed) contours denote positive (negative) values, and the zero contour is suppressed.

of the NPO/WP signal, indicating that these patterns are in quadrature. The ENSO SLP has more overlap with the PNA pattern than NPO/WP. But the ENSO and PNA signals are still quite distinct with the ENSO signal focused in the Gulf of Alaska and the PNA signal in the shadow of the Aleutians. [See Nigam (2003) for a more in-depth intercomparison.] The PNA and NPO/WP impact on the Asian–Pacific jet has been noted before (cf. Fig. 5).

The PNA influence on North American hydroclimate is shown in the left column of Fig. 11. In contrast with the NPO/WP signal, precipitation is diminished everywhere from the Aleutians to the Pacific Northwest except for a very narrow zone along the Alaskan Gulf. The impact on the United States is very different as well: Precipitation is strongly suppressed in the eastern part with the exception of Florida while there is no impact on the southwest region and the central Great

Plains, two areas significantly influenced by NPO/WP variability.

The ENSO precipitation impact is well documented and discussed in the literature (e.g., Ropelewski and Halpert 1986; Green et al. 1997) and is displayed here, only for contextual reference. The broad similarity with the NPO/WP impact, especially over the southern United States, is noteworthy, notwithstanding the extensive enhancement of precipitation over the southeastern states, including Florida, during El Niño winters.

The PNA SAT impact on Alaska, Canada, and the Pacific Northwest bears striking resemblance to the NPO/WP warming signal (cf. Fig. 8b) in view of southerly flow in both cases: south/southeasterly in case of the PNA and southwesterly in NPO/WP variability. The PNA trough is more expansive, skirting the U.S. coast and leading to warmer temperature over the western states as well.⁷ The PNA warming however does not extend to the eastern seaboard, as in case of NPO/WP variability, a result that can again be understood from consideration of anomalous thermal advection. Although bearing some structural similarity, the ENSO SAT signal is rather muted in comparison with the other two on account of weaker circulation impact over the American continent (see Nigam 2003).

The above intercomparison reveals that NPO/WP variability exerts profound influence on the Alaskan, Pacific Northwest, Canadian and U.S. winter surface air temperatures, more so than PNA or ENSO. The NPO/WP variability is likewise more influential on the Pacific Northwest, western Mexico, and south-central Great Plains winter precipitation. Although, NPO/WP variability has not been extensively analyzed, it is, evidently, as, if not more, consequential for the North American winter climate.

7. Comparisons with NAO

The NAO and NPO/WP share many structural similarities, leading to the notion of dynamical analog (Nigam 2003, see his Fig. 17 and attendant discussion). A somewhat more extensive intercomparison of the two modes of winter variability is undertaken here in the interest of furthering insight into NPO/WP origin and evolution.

The NAO is diagnosed here just as the NPO/WP was: unrotated, covariance-based EOF analysis of area-

weighted winter monthly SLP anomalies over the Atlantic basin (20° – 85° N, 80° W– 0°). The first EOF closely resembles the NAO pattern; its PC is correlated with Hurrell's (1995) NAO index at 0.93.

Both SLP patterns exhibit a meridional dipole consisting of a zonally elongated band in the subtropics and a center near 60° N (Fig. 13; note map rotation). A third center having the same sign as the subtropical center is present $\sim 180^{\circ}$ of longitude away in both cases. The NAO pattern has almost twice the amplitude though. The 500-hPa regressions are strikingly similar as well, with both patterns exhibiting vertical coherence and equivalent barotropic vertical structure.

The NPO/WP and NAO patterns are located near the exit region of the Asian–Pacific and Atlantic jets, respectively (cf. Fig. 14, left panels). The 300-hPa zonal wind anomalies are displayed atop the climatological jets in this figure, and the significance of the NAO anomaly is readily apparent. Not only is this anomaly twice as large, as noted earlier, it is superposed on a climatological jet that is three times weaker, making NAO perturbations very effective in jet modulation; perhaps, a factor of 6 more than for the NPO/WP. The dipolar anomalies shift the jet poleward and extend it eastward as well, evidently much more in the NAO case.

A troposphere-wide view of jet variability is provided in the right panels, which show the climatological and anomalous zonal wind averages in the Pacific (120° E– 120° W) and Atlantic (80° W– 0°) sectors. The sector-averaged wind anomalies straddle the climatological jet core in both cases, rather precisely in the NPO/WP case. However, the anomalies are stronger and considerably more effective in the NAO case for reasons stated earlier.

To be sure, there are some differences between these variability modes too. While both primarily involve a poleward shift and eastward extension of the respective jets, the NAO zonal wind anomalies contain extra features in the tropics and polar regions, albeit of weak amplitude. This difference notwithstanding, the remarkable similarity in the mature-phase structure of the modes suggests similar genesis and spatiotemporal evolution. Analysis of weekly data is underway to investigate these issues.

8. Discussion

This study presents a refined description of the North Pacific Oscillation (in winter sea level pressure) and its upper-air signature, the west Pacific teleconnection pattern. The surface variability pattern has been known for almost a century (since 1916, see Walker and Bliss

⁷ Note, warmer SATs may also result from zonal advection since southerly flow along the coast will lead to Ekman downwelling and warmer coastal SSTs. Climatological westerlies can then produce warm advection.

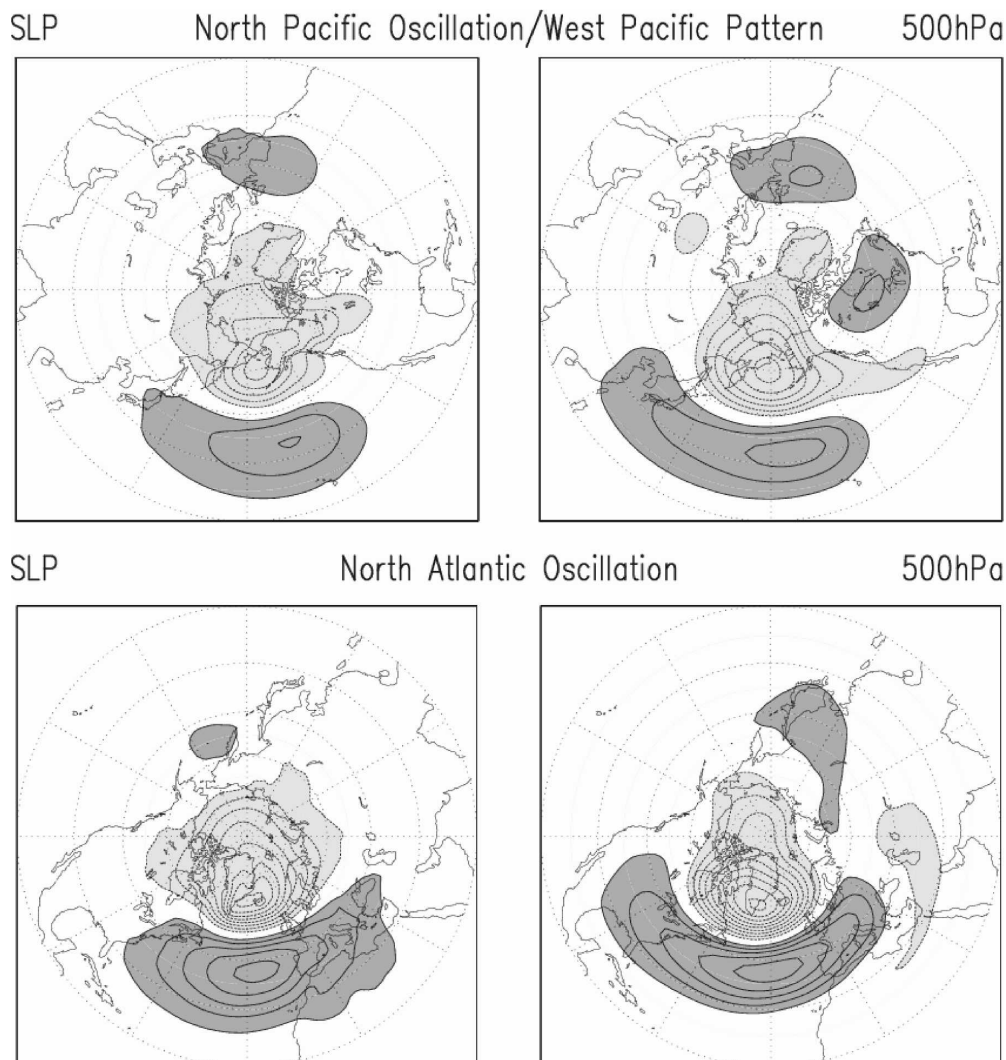


FIG. 13. Winter sea level pressure and 500-hPa height patterns associated with (top) NPO/WP and (bottom) NAO variability in the 1958–2001 winter months in the ERA-40 dataset. Contour/shading interval is 1.0 hPa for SLP and 10 m for geopotential height; solid (dashed) contours denote positive (negative) values, and the zero contour is suppressed. Note the map rotation between top and bottom panels.

1932), and with the NPO naming since 1932. Yet, and despite its origin as a North American weather-influencing pattern in the far upstream region (with predictability implications), only a handful of studies have sought to further characterize the NPO structure and impacts in the intervening decades (WG81; Rogers 1981; Lau 1988; Nigam 2003). This is in stark contrast with the North Atlantic Oscillation, a basin analog of the NPO [a case made in Nigam (2003) and here], which has been more extensively studied because of its European weather and climate impacts (e.g., Hurrell et al. 2006).

The present study reports on the first part of a project that seeks to advance understanding of NPO/

WP's spatiotemporal structure, variability mechanism(s), and Arctic sea ice and North American hydroclimate impacts. The mature phase of variability is targeted first because it is easily identified in monthly averages, which are readily available; it fosters intercomparison with previous studies that are, by and large, based on monthly data and because robust impacts anticipated in the mature phase can provide rationale and motivation for the subsequent weekly resolution and evolution-focused analysis.

The principal findings of the study are as follows:

- The North Pacific Oscillation and west Pacific teleconnection pattern are two faces of the same variabil-

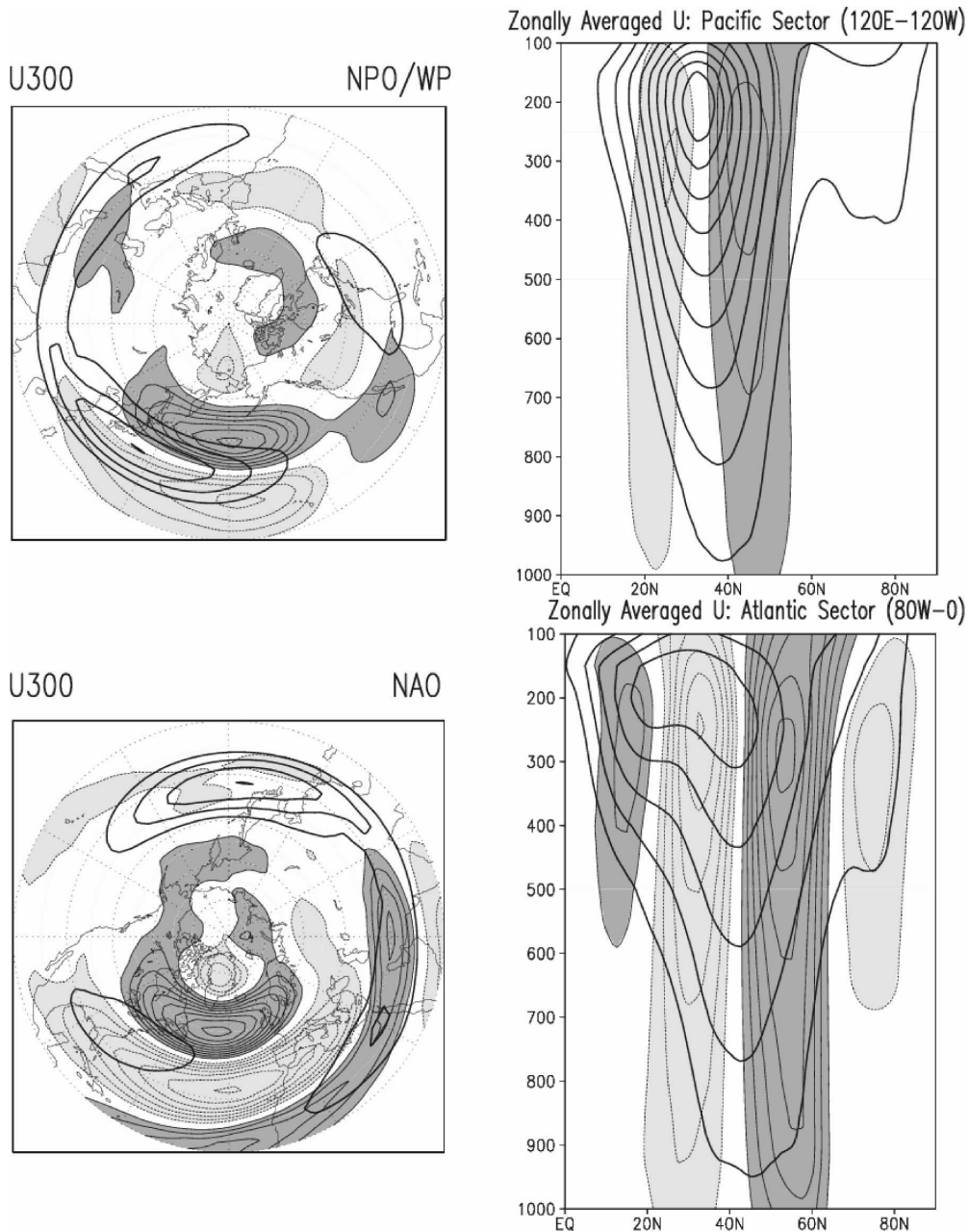


FIG. 14. Zonal wind patterns associated with (top) NPO/WP and (bottom) NAO variability in the 1958–2001 winter months (DJFM) in the ERA-40 dataset. The corresponding zonal wind climatology is superposed using thick contours. (left) The 300-hPa regressions (contoured/shaded at 1 m s^{-1} interval) and climatology (starting at 30 m s^{-1} , with an interval of 10 m s^{-1}). (right) Latitude–height cross sections of the Pacific sector (120°E – 120°W) and Atlantic sector (80°W – 0°) average flow. Cross-section regressions are contoured/shaded with a 1 m s^{-1} interval, while sector climatology is contoured with a 5 m s^{-1} interval. Note the map rotation between upper- and lower-left panels.

ity mode, the NPO/WP. While this link has been noted before (WG81; Hsu and Wallace 1985; Nigam 2003), it has hitherto not been firmly established from consistent analysis of long data records.

- The NPO/WP is very influential on marginal ice zone extent in the Arctic seas, with the western Bering Sea

and Sea of Okhotsk ice zones significantly extended during the positive NPO/WP phase. The influence on the Arctic MIZ extent surpasses that of other Pacific variability modes (PNA, ENSO).

- The NPO/WP exerts substantial influence on North American hydroclimate, leading to continent-wide

warming and increased precipitation along the Alaskan/Canadian coast and over the south-central Great Plains. The hydroclimate impact is, at least, as significant as the winter PNA and ENSO impacts in these regions.

- The NPO/WP is a basin analog of the NAO: both exhibit similar dipolar SLP anomalies, perturb the climatological jet in their basin sectors similarly, and are connected to storm track modulation (Lau 1988). The parallel structure suggests that similar dynamical mechanisms may be operative as well, raising the possibility of dynamical analogs.

Monthly analysis provides valuable insight into the mature-phase structure but little into variability evolution, that is, genesis and decay of NPO/WP variability. As noted before, the NPO/WP is, primarily, a subseasonal mode of variability, making monthly means too coarse for resolving NPO/WP evolution. As such, weekly averaged anomalies have been generated to study evolution, including nascent and decay phases and the underlying mechanisms.

A weekly analysis is also motivated by interest in understanding how the monthly MIZ impact is generated, in particular, the rectified effects of weekly sea ice and thermal advection anomalies. MIZ variability also impacts turbulent heat, moisture, and momentum fluxes at the air–sea interface, which, in turn, can influence cyclogenesis and cyclone tracks and, thus, the storm track system.

Weekly analysis will address variability genesis but, above all, provide context for investigating the NPO/WP-based predictability of Arctic sea ice and North American winter hydroclimate variability, seeking to fill the void between extended-range weather and monthly/seasonal climate predictions.

Acknowledgments. We thank Alfredo Ruiz-Barradas, Scott Weaver, and Steven Chan for help with datasets and aspects of data analysis. Dan Vimont and another reviewer (anonymous), and editor Clara Deser, provided comprehensive and constructive reviews, which are gratefully acknowledged. The authors wish to thank Adam Phillips and Clara Deser of NCAR for providing the satellite-based sea ice data in a user-friendly gridded format. The authors wish to acknowledge support of Grants NOAA/CPPA NA17EC1483 and NSF ATM-0649666. The first author also thanks Andrew Durante for constructive suggestions.

REFERENCES

- Barnston, A. G., and R. E. Livezey, 1987: Classification, seasonality and persistence of low-frequency atmospheric circulation patterns. *Mon. Wea. Rev.*, **115**, 1083–1126.
- Cavaliere, D. J., and C. L. Parkinson, 1987: On the relationship between atmospheric circulation and fluctuations in the sea ice extents of the Bering and Okhotsk seas. *J. Geophys. Res.*, **92**, 7141–7162.
- , —, P. Gloerson, and H. J. Zwally, 2006: Sea ice concentrations from Nimbus-7 SMMR and DMSP SSM/I passive microwave data. National Snow and Ice Data Center, Boulder, CO, digital media. [Available online at http://nsidc.org/data/docs/daac/nsidc0051_gsfc_seaice.gd.html.]
- Cayan, D. R., 1992: Latent and sensible heat flux anomalies over the northern oceans: The connection to monthly atmospheric circulation. *J. Climate*, **5**, 354–369.
- Chaing, J. C. H., and D. J. Vimont, 2004: Analogous Pacific and Atlantic meridional modes of tropical atmosphere–ocean variability. *J. Climate*, **17**, 4143–4158.
- Chang, E. K. M., 1993: Downstream development of baroclinic waves as inferred from regression analysis. *J. Atmos. Sci.*, **50**, 2038–2053.
- , S. Lee, and K. L. Swanson, 2002: Storm track dynamics. *J. Climate*, **15**, 2163–2183.
- Esbensen, S. K., 1984: A comparison of intermonthly and interannual teleconnections in the 700 mb geopotential height field during Northern Hemisphere winter. *Mon. Wea. Rev.*, **112**, 2016–2032.
- Fang, Z., and J. M. Wallace, 1994: Arctic sea ice variability on a timescale of weeks and its relation to atmospheric forcing. *J. Climate*, **7**, 1897–1914.
- Feldstein, S. B., 2000: The timescale, power spectra, and climate noise properties of teleconnection patterns. *J. Climate*, **13**, 4430–4440.
- Fissel, D. B., and C. L. Tang, 1991: Response of sea ice drift to wind forcing on the northeastern Newfoundland shelf. *J. Geophys. Res.*, **96**, 18 397–18 409.
- Green, P. M., D. M. Legler, C. J. Miranda V., and J. J. O'Brien, cited 2007: The North American climate patterns associated with El Niño–Southern Oscillation. COAPS Project Report Series 97–1. [Available online at <http://www.coaps.fsu.edu/lib/booklet/>.]
- Guan, B., and S. Nigam, 2008: Pacific sea surface temperatures in the twentieth century: An evolution-centric analysis of variability and trend. *J. Climate*, in press.
- Horel, J. D., 1981: A rotated principal component analysis of the interannual variability of the Northern Hemisphere 500 mb height field. *Mon. Wea. Rev.*, **109**, 2080–2092.
- Hoskins, B. J., H. H. Hsu, I. N. James, M. Masutani, P. D. Sardeshmukh, and G. H. White, 1989: Diagnostics of the global atmospheric circulation, based on ECMWF analyses 1979–1989. WCRP-27, WMO Tech. Doc. 326, 217 pp.
- Hsu, H.-H., and J. M. Wallace, 1985: Vertical structure of wintertime teleconnection patterns. *J. Atmos. Sci.*, **42**, 1693–1710.
- Hurrell, J. W., 1995: Decadal trends in the North Atlantic Oscillation: Regional temperatures and precipitation. *Science*, **269**, 676–679.
- , and Coauthors, 2006: Atlantic climate variability and predictability: A CLIVAR perspective. *J. Climate*, **19**, 5100–5121.
- Johnson, C. M., 1980: Wintertime Arctic sea ice extremes and the simultaneous atmospheric circulation. *Mon. Wea. Rev.*, **108**, 1782–1791.
- Kutzbach, J. E., 1970: Large-scale features of monthly mean Northern Hemisphere anomaly maps of sea-level pressure. *Mon. Wea. Rev.*, **98**, 708–716.
- Lau, N.-C., 1988: Variability of the observed midlatitude storm

- tracks in relation to low-frequency changes in the circulation pattern. *J. Atmos. Sci.*, **45**, 2718–2743.
- , and M. J. Nath, 1991: Variability of the baroclinic and barotropic transient eddy forcing associated with monthly changes in the midlatitude storm tracks. *J. Atmos. Sci.*, **48**, 2589–2613.
- Mitchell, T. D., and P. D. Jones, 2005: An improved method of constructing a database of monthly climate observations and associated high-resolution grids. *Int. J. Climatol.*, **25**, 693–712.
- Nigam, S., 1994: On the dynamical basis for the Asian summer monsoon rainfall–El Niño relationship. *J. Climate*, **7**, 1750–1771.
- , 2003: Teleconnections. *Encyclopedia of Atmospheric Sciences*, J. R. Holton et al., Eds., Academic Press, 2243–2269.
- , and E. DeWeaver, 2003: Stationary waves (orographically and thermally forced). *Encyclopedia of Atmospheric Sciences*, J. R. Holton et al., Eds., Academic Press, 2121–2137.
- , and A. Ruiz-Barradas, 2006: Seasonal hydroclimate variability over North America in global and regional reanalyses and AMIP simulations: Varied representation. *J. Climate*, **19**, 815–837.
- , C. Chung, and E. DeWeaver, 2000: ENSO diabatic heating in ECMWF and NCEP reanalyses, and NCAR CCM3 simulation. *J. Climate*, **13**, 3152–3171.
- Orlanski, I., 2005: A new look at the Pacific storm track variability: Sensitivity to tropical SSTs and to upstream seeding. *J. Atmos. Sci.*, **62**, 1367–1390.
- Parkinson, C. L., and A. J. Gratz, 1983: On the seasonal sea ice cover of the Sea of Okhotsk. *J. Geophys. Res.*, **88**, 2793–2802.
- Pease, C. H., 1980: Eastern Bering Sea ice processes. *Mon. Wea. Rev.*, **108**, 2015–2023.
- Prinsenbergh, S. J., I. K. Peterson, S. Narayanan, and J. U. Umoh, 1997: Interaction between atmosphere, ice cover, and ocean off Labrador and Newfoundland from 1962–1992. *Can. J. Fish Aquat. Sci.*, **54**, 30–39.
- Rayner, N. A., D. E. Parker, E. B. Horton, C. K. Folland, L. V. Alexander, D. P. Rowell, E. C. Kent, and A. Kaplan, 2003: Global analyses of sea surface temperature, sea ice, and night marine air temperature since the late nineteenth century. *J. Geophys. Res.*, **108**, 4407, doi:10.1029/2002JD002670.
- Renwick, J. A., and J. M. Wallace, 1996: Relationships between North Pacific blocking, El Niño, and the PNA pattern. *Mon. Wea. Rev.*, **124**, 2071–2076.
- Rogers, J. C., 1981: The North Pacific Oscillation. *J. Climatol.*, **1**, 39–57.
- , 1990: Patterns of low-frequency monthly sea level pressure variability (1899–1986) and associated wave cyclone frequencies. *J. Climate*, **3**, 1364–1379.
- Ropelewski, C. F., and M. S. Halpert, 1986: North American precipitation and temperature patterns associated with the El Niño/Southern Oscillation (ENSO). *Mon. Wea. Rev.*, **114**, 2352–2362.
- Schevchenko, G. V., A. B. Rabinovich, and R. E. Thomson, 2004: Sea-ice drift on the northeastern shelf of Sakhalin Island. *J. Phys. Oceanogr.*, **34**, 2470–2491.
- Solomon, S., D. Qin, M. Manning, Z. Chen, M. Marquis, K. B. Averyt, M. Tignor, and H. L. Miller, Eds., 2007: *Climate Change 2007: The Physical Science Basis*. Cambridge University Press, 940 pp.
- Thorndike, A. S. and R. Colony, 1982: Sea ice motion in response to geostrophic winds. *J. Geophys. Res.*, **87**, 5845–5852.
- Uppala, S. M., and Coauthors, 2005: The ERA-40 Re-Analysis. *Quart. J. Roy. Meteor. Soc.*, **131**, 2961–3012.
- Vimont, D. J., D. S. Battisti, and A. C. Hirst, 2003a: The seasonal footprinting mechanism in the CSIRO general circulation models. *J. Climate*, **16**, 2653–2667.
- , J. M. Wallace, and D. S. Battisti, 2003b: The seasonal footprinting mechanism in the Pacific: Implications for ENSO. *J. Climate*, **16**, 2668–2675.
- Walker, G. T., and E. W. Bliss, 1932: World weather V. *Mem. Roy. Meteor. Soc.*, **4**, 53–84.
- Wallace, J. M., and D. S. Gutzler, 1981: Teleconnections in the geopotential height field during the Northern Hemisphere winter. *Mon. Wea. Rev.*, **109**, 784–812.